RSC Advances

PAPER

View Article Online
View Journal | View Issue

Cite this: *RSC Adv.*, 2024, **14**, 27816

Amelioration of gold nanoparticles mediated through *Ocimum* oil extracts induces reactive oxygen species and mitochondrial instability against MCF-7 breast carcinoma

Yugal Kishore Mohanta, †[ab] Kunal Biswas,†[c] Awdhesh Kumar Mishra,†[d] Biswajit Patra,[e] Bishwambhar Mishra,[f] Jibanjyoti Panda,[a] Satya Kumar Avula,[g] Rajender S. Varma,[h] Bibhu Prasad Panda *[i] and Debasis Nayak*[j]

Phytomedicines are potential immunity-boosting components with effective anticystic properties, minimal side effects, and biomedical applications, making them valuable for combating various diseases. India is renowned globally for Ayurveda, an ancient treatment methodology known for its holistic approach in identifying the root cause of diseases. Tulsi (*Ocimum sanctum*) is a common household medicine in India. While essential oils from plants like Tulsi have long been recognized for their medicinal properties, there is a gap in understanding their potential in synthesizing gold nanoparticles (AuNPs) and their efficacy against breast carcinoma, particularly in the context of immunosuppressive conditions. We investigated the potential application of essential oils isolated from *O. sanctum* in the synthesis of AuNPs and their efficacy against MCF-7 breast carcinoma. Gas chromatography-mass spectroscopy identified compounds with potential anticancer effects against breast cancer cells. Synthesised AuNPs displayed high hemocompatibility and antimicrobial activity against nosocomial *Pseudomonas aeruginosa*, *Escherichia coli*, *Vibrio cholerae*, and *Bacillus subtilis* strains. Os-AuNPs induced chromosomal instability and mitotic arrest in the G2/M cell cycle phase. Subsequent fluorescence and cell cytometry studies demonstrated the systemic release of ROS, depolarisation of mitochondrial membrane potential, and production of apoptotic bodies. DNA damage and comet assays confirmed the anticancer potential of synthesised AuNPs. This study illuminates the potential of *O. sanctum*-derived AuNPs in breast carcinoma treatment, paving the way for future AuNP-based therapies in biomedicine.

Received 2nd July 2024
Accepted 20th August 2024

DOI: 10.1039/d4ra04807e

rsc.li/rsc-advances

[a]*Nano-biotechnology and Translational Knowledge Laboratory, Department of Applied Biology, School of Biological Sciences, University of Science and Technology Meghalaya, Techno City, 9th Mile, Baridua, Ri-Bhoi 793101, Meghalaya, India*

[b]*Centre for Herbal Pharmacology and Environmental Sustainability, Chettinad Hospital and Research Institute, Chettinad Academy of Research and Education, Kelambakkam 603103, Tamil Nadu, India*

[c]*Centre for Nanoscience & Nanotechnology International Research Centre, Sathyabama Institute of Science and Technology, Jeppiaar Nagar, Rajiv Gandhi Salai, Chennai 600119, India*

[d]*Department of Biotechnology, Yeungnam University, Gyeongsan 38541, South Korea*

[e]*Department of Botany, Fakir Mohan University, Balasore 756020, Odisha, India*

[f]*Department of Biotechnology, Chaitanya Bharathi Institute of Technology (CBIT), Gandipet, Hyderabad 500075, Telangana, India*

[g]*Natural and Medical Sciences Research Centre, University of Nizwa, Nizwa 616, Oman*

[h]*Centre of Excellence for Research in Sustainable Chemistry, Department of Chemistry, 20 Federal University of São Carlos, 13565-905 São Carlos, SP, Brazil*

[i]*Environmental Sciences, Department of Chemistry, ITER, Siksha "O" Anusandhan (Deemed to be University), Bhubaneswar 751030, Odisha, India. E-mail: bibhuprasadpanda@soa.ac.in*

[j]*Bioresources and Traditional Knowledge Laboratory, Department of Wildlife and Biodiversity Conservation, Maharaja Sriram Chandra Bhanja Deo University, Sriram Chandra Vihar, Takatpur, Baripada 757003, India. E-mail: deb63nayak@gmail.com*

† Authors contributed equally.

1 Introduction

With the surge in disease miscellany, prognosis, and development of multiple drug-resistant microorganisms, the search for novel bioactive components and pharmaceutically active molecules has augmented research in national and international forums. Various pharmaceutically active phytochemicals, such as alkaloids, amines, phenols, terpenoids, polyphenols, quinones, and essential oils, have been isolated and characterised. Plants and their secondary metabolites have been used to treat various ailments in humans, cattle, and in agricultural practices since the medieval period.[1–4] These phytochemicals function as defence tactics for plants, as they have evolved over time to interfere with the metabolism, neuronal transmission, and reproduction of interacting microorganisms or predators such as herbivores.[5,6] A large number of pharmacologically active compounds used as herbal medicines exhibit a positive correlation with their modern pharmaceutical drug counterparts.[7] One group of such secondary metabolites is essential oils, which are volatile components responsible for the aroma of

plants and defence mechanisms against invading microbial agents.[8,9] They can be described as plant-derived hydrophobic, organic, and less viscous volatile oils that are colourless and possess distinctive and specific odours or fragrances with water-like textures.[10,11] Essential oils are found in almost every part of the plant and are primarily produced to protect it from invading pests, bacteria, fungi, viruses, and potential predators. The fragrance of essential oils also promotes pollination by attracting insects.[12]

Species of the Lamiaceae family are autochthonous plants that are distributed worldwide. They have been used traditionally for centuries in culinary activities as flavouring agents, fragrances, and food preservatives, and most significantly, for their medicinal properties.[13,14] The most noteworthy and largest genera of the Lamiaceae family is the genus *Ocimum* which is considered as the "Grand Master Herb" or the "King of Herbs.[15] Tulsi (*Ocimum sanctum*) commonly known as the "Holy basil" is native to India and widely distributed all over the Asian subcontinent. In Ayurveda, it has been considered a "Life tonic" as it provides solutions for various ailments, including common cold, cough, headache, stomach disorder, inflammation, antiseptic, malaria, asthma, and conjunctivitis.[16–18] The essential oils present in Tulsi have been widely accepted to boost immunity and are considered a part of herbal tea during Covid-19.[19–21]

The global Cancer Observatory, under the guidance of the International Agency for Research on Cancer (IARC) of the World Health Organization, estimated that ~17.4% of the female population in India had breast carcinoma in 2020 (GLOBOCAN 2020). Surgery and subsequent chemotherapy sessions provide facultative bacteria and other microorganisms with a golden opportunity to invade patients with immunosuppressive breast cancer. The use of nanoparticles in various ointments and therapeutics has been well documented.[22] Biological synthesis of metallic nanoparticles provides novel approach for the bio-fabrication of metallic salts and their components compared to the chemically synthesized nanomaterials. Herein, a simple and cost-effective method for synthesising AuNPs biologically from essential oils of *Ocimum sanctum* oil extracts is described, including the exploration of their anticancer and antimicrobial activities through cell cycle analysis and mitochondrial membrane potential destabilisation studies. The effects of AuNPs on the DNA machinery of cancer cells were demonstrated using DNA fragmentation, comet formation, and colony formation assays. The synergistic effect of *Ocimum sanctum*-synthesised gold nanoparticles (Os-AuNPs) and essential oils from *Ocimum sanctum* against MCF-7 breast cancer cells may be useful for the transdermal delivery of pharmacologically active nanoformulations using novel gels or formulations.

2 Materials and methods

Hydrogen tetrachloroaurate(III) trihydrate ($HAuCl_4 \cdot 3H_2O$), 3-[4,5-dimethylthiazol-2-yl]-2,5-diphenyl tetrazolium bromide (MTT), 2,2-diphenyl-1-picrylhydrazyl (DPPH), Dulbecco's modified Eagle's medium (DMEM), Rhodamine 123, and Propidium iodide were procured from Sigma-Aldrich, USA. Nutrient agar, Nutrient broth, and different analytical-grade chemicals were purchased from Merck, India.

2.1. Collection and preparation of extract

Ocimum sanctum leaves were collected from the herbal garden of University of Science and Technology Meghalaya, India. The leaves were rinsed with Millipore water to remove dust and subjected to hydro distillation using a Soxhlet apparatus (Borosil) for 3 h. The obtained methanolic extract was subsequently fractionated by column chromatography. The obtained oil was subjected to Gas Chromatography (GC 2400™ PerkinElmer, USA) for compound identification and was stored at 4 °C for further characterisation.

2.2. Gas chromatography-mass spectroscopy (GC-MS) of *O. sanctum* essential oil

The oil extract of *O. sanctum* was analysed to detect various pharmaceutically active compounds using the standard protocol for GC-MS.[23] Briefly, 40 μL of methoxyamine hydrochloride (MeOX) was added to the oil extract and incubated for 2 h at 60 °C. Later, 80 μL of mono-trimethylsilyl-trifuoroacetamide (MSTFA) was added to it and was further incubated for 1 h. Before GC-MS analysis, the samples were centrifuged, and the supernatant was collected for data acquisition.[24,25]

2.3. Green synthesis of gold nanoparticles by the *O. sanctum* essential oils (Os-AuNPs)

AuNPs were prepared according to a method previously reported by our group.[26] Briefly, to synthesise the Os-AuNPs, 10 mL of diluted *O. sanctum* essential oil was added to 90 mL of 1.0 mM aq. $HAuCl_4 \cdot 3H_2O$ solution to obtain AuNPs. The subsequent change in the reaction mixture from brownish to ruby-red/wine red provided the primary inference of the biological reduction of the $HAuCl_4 \cdot 3H_2O$ salt to AuNPs. Finally, the Os-AuNPs were centrifuged at 10 000 rpm for 30 min. The obtained pellets were rinsed thrice with distilled water and centrifuged. Finally, the obtained pellets were lyophilised and stored at 4 °C for further characterisation.

2.4. Characterization of the synthesized Os-AuNPs

The synthesised Os-AuNPs were scanned using a UV-Vis spectrophotometer (UV-5704SS double-beam spectrophotometer) in the wavelength range of 300–800 nm. Dynamic light scattering (DLS) was performed to determine the overall size and charge of the bio-reduced Os-AuNPs. Briefly, the synthesised Os-AuNPs were dispersed in water *via* water bath sonication and analysed using a Zetasizer (ZS 90, Malvern, UK). The surface size and composition of the synthesised Os-AuNPs were examined using scanning electron microscopy (SEM) (Lyra3 TESCAN VEGA3) and transmission electron microscopy (TEM) (JEOL 2100F) at 200 kV. The Os-AuNPs were adhered to glass slides and coated with gold using a gold-sputter module in a high-vacuum evaporator. Energy Dispersive X-ray spectroscopy

(EDX) was used to scan the elemental constituents of the Os-AuNPs. XRD patterns were captured using an X-ray diffractometer (PANalytical X'Pert, Almelo, Netherlands) fitted with a Ni filter and radiation source of Cu Kα ($l = 1.54056$ Å). The 2θ angle was varied within 10–90° at a scanning rate of 0.05° s^{-1}. Attenuated total reflection Fourier-transform infrared (ATR-FTIR) spectroscopy was used to investigate the surface modification of the synthesised nanoparticles. At a resolution of 4 cm^{-1} and spectral region of 4000–500 cm^{-1}, the samples were scanned using ATR-FTIR (Bruker ALPHA, Ettlinger, Germany).

2.5. Hemocompatibility assay

A potential hemolytic activity test of the green-synthesised Os-AuNPs was performed using a standard protocol with slight modifications.[27] Briefly, blood was collected from healthy volunteers and mixed with normal saline (NS) buffer. Accordingly, 200 μL (1 mg mL^{-1}) of Os-AuNPs was added to 5 mL of NS followed by addition of 0.2 mL diluted blood. The mixture was incubated for 1 h at 30 °C and was later centrifuged at 1000 rpm for 5 min. The optical density (OD) of the supernatant was measured at 540 nm using a UV-Vis spectrophotometer. 0.1% sodium carbonate was used as a positive control, and normal saline was used as the negative control.

$$\text{Hemolysis (\%)} = \frac{OD_t - OD_{nc}}{OD_{pc} - OD_{nc}} \quad (1)$$

2.5.1. Hemagglutination assay. The hemagglutinin activity of the Os-AuNPs was determined according to a standard protocol.[28] Briefly, In a 96 "U"-shaped plate, 100 μL of NS was added to each well. The 1st column served as the (−)ve control, containing only RBCs and NS. On the other hand, the 12th column served as a (+) ve control, containing only sodium carbonate and RBCs. In all wells, 1 mg mL^{-1} Os-AuNPs was serially diluted from well 2 to well 11, and at last diluted RBCs (100 μL) were added to each well. After 2 h of incubation, a button-like morphology was observed.

2.6. Antibacterial activity

The agar well assay and minimum inhibitory concentration (MIC) activity of Os-AuNPs were conducted using nosocomial strains of *Pseudomonas aeruginosa* (MTCC 1688), *Escherichia coli* (MTCC 1098), *Vibrio cholerae* (MTCC 3904), and *Bacillus subtilis* (MTCC 1427). Bacteria were obtained from the Microbial Type Culture Collection (MTCC), Chandigarh, India. Isolated colonies of the test organism were injected into 20 mL of sterile MHB (Mueller Hinton Broth, 95% purity), and the mixture was cultured at 37 °C for 24 h. After incubation, a sterile glass rod spreader was used to transfer the turbid test culture to the MHA plates, and a sterile cork borer was used to create wells in each plate. Finally, 100 μL of an aqueous solution of Os-AuNPs at a concentration of 100 μg mL^{-1} was added to each well, and the plates were incubated for 24 h at 37 °C. The standard antibiotic Gentamycin was used as positive control. Furthermore, the micro broth dilution (MBD) method was used to assess the minimum inhibitory concentration (MIC) of Os-AuNPs on bacterial strains.[29] Microbial growth and inhibition were measured at 600 nm using a Microplate Reader (Bio-Rad) in 96-well plates. IC_{50}/IC_{90} Laboratory Excel Calculation Tools were used to determine the MIC, which was then converted to IC_{50} values. Each experiment was performed three times to ensure accurate results, and the percentage of inhibition was reported using the mean standard deviation.

2.7. MTT assay

The cell viability and proliferative activity of the Os-AuNPs were determined using the MTT assay following a standard protocol.[30] Briefly, MCF-7 cells (a Breast Cancer cell line) were procured from NCCS (Pune, India) and grown using Dulbecco's Modified Eagle Medium (DMEM) supplemented with 10% Fetal Bovine Serum (FBS) and 1% antibiotic solution (Penicillin/Streptomycin), in a 5% CO_2 incubator, at 37 °C. Briefly, the cells were grown up to 96 well plates for 70% confluency and then different concentrations (10–200 μg mL^{-1}) of Os-AuNPs were incubated with MCF-7 cells for 24 h. Later, 100 μL of MTT (5 mg mL^{-1}) was added to the 96 well plates and incubated for 4 h. Subsequently, after discarding the MTT solution, 100 μL of DMSO was added and incubated for 15 min. Finally, the OD was measured at 595 nm (2030 Multilabel Processor Victor™X3, PerkinElmer, USA).

2.8. Cell cycle analysis by flow cytometer

The effect of the Os-AuNPs on the cell cycle of MCF-7 breast cancer cells was analysed by flow cytometry using a standard protocol.[31] The MCF-7 cells after treatment with Os-AuNPs were processed and stained with Propidium Iodide (PI) dye. After staining, the cells were incubated at 4 °C for 30 min and analysed using a BD Accuri C6 flow cytometer (BD Biosciences).

2.9. Detection of total ROS activity

The total ROS activity of Os-AuNP-treated MCF-7 cells was measured using a standard dichlorodihydrofluorescein diacetate (DCFH-DA) dye, following a standard protocol.[32] Total internal Reactive Oxygen Species were monitored by flow cytometry using an FL-1 filter, and fluorescent images were captured using an Epi-fluorescence microscope (Olympus IX71, Olympus, Tokyo, Japan).

2.10. Mitochondrial membrane potential analysis

To estimate the mitochondrial membrane potential of Os-AuNP-treated MCF-7 breast cancer cells using flow cytometry and fluorescence microscopy, a Rhodamine 123 assay was performed following the standard protocol.[33] The fluorescence intensity of nanoparticle-treated cells after incubation with 10 mM Rhodamine 123 (Rh 123) dye was measured using flow cytometry. For fluorescence microscopy imaging, Rh 123 stained cells were fixed with paraformaldehyde and images were captured using an epi-fluorescence microscope.

2.11. DNA-AuNPs interaction studies

DNA-AuNP interaction studies were performed to assess the DNA damage caused by incubation with Os-AuNPs.[34] Briefly,

after treatment with Os-AuNPs, MCF-7 cells were harvested and processed for 1.5% gel electrophoresis. Fragmented DNA bands were visualised using a gel documentation system (Bio-Rad, India). A comet assay was performed to detect the amelioration of DNA at the single-cell stage. The Os-AuNP-treated MCF-7 cells were harvested and processed with low-melting agarose, followed by electrophoresis. The slides were then stained with PI dye, and images were captured using an Epi fluorescent microscope. Various comet parameters were analysed using ImageJ Open Comet.

2.12. Annexin V-FITC staining

Annexin V-FITC staining of Os-AuNP-treated MCF-7 cells was performed to categorise the nanoparticle-induced death mechanism following a standard protocol.[27] Briefly, nanoparticle-treated cells were harvested by trypsinisation and centrifugation. The resulting pellet was washed and incubated in Annexin V-binding buffer (100 μL) and Annexin V-FITC (5 μL) for 15 min. The samples were further centrifuged, the pellet was resuspended in binding buffer (200 μL), and before analysis, PI dye (5 μL) was added and scanned on a BD Accuri C6 flow cytometer with emission filters of 495–520 nm for FITC (green) and 600 nm for PI (red).

2.13. Colony forming assay

An *in vitro* clonogenic assay was performed according to a standard protocol.[34] Briefly, in a six-well plate, MCF-7 breast cancer cells were treated with Os-AuNPs, and after 14 days, they were stained (crystal violet and glutaraldehyde), and the colonies were counted after air drying.

2.14. Statistical analysis

Statistical significance of the data was determined using Duncan's test. All data are presented as mean ± standard deviation (SD). Data were considered statistically significant at $p < 0.05$. All experiments were performed in triplicate.

3 Results and discussion

3.1. GC-MS analysis

Aromatic plants are known to be a storehouse of diverse array of essential oils. *O. sanctum* widely known as Tulsi is well known for its medicinal properties has high accumulation of essential oils. In the current investigation, the GC-MS analysis of the oil extracts demonstrated the presence of benzene, 1,2-dimethoxy-4-(2-propenyl) – (synonym: methyl isoeugenol), isocaryophyllene (synonym: caryophyllene), and eugenol (synonym: 2-methoxy 4-(2-propenyl) phenol). Fig. 1 shows the GC-MS chromatogram of the major components of the *O. sanctum* oil extracts.

3.2. Synthesis and characterization of Os-AuNPs

Colour change was the first visible observation that indicated the synthesis of nanoparticles.[26] In this study, essential oils were obtained from the leaf extracts of *Ocimum sanctum*, commonly known as holy basil, in India. Upon the addition of $HAuCl_4$, the colour of the solution rapidly changed from brownish yellow to ruby wine red, indicating the reduction of the $HAuCl_4$ salt to AuNPs. This colour change is primarily due to a phenomenon called surface plasmon resonance (SPR) which is generally caused by a change in the surface-to-volume ratio of the synthesised nanoparticles. The synthesised Os-AuNPs were scanned using a UV-Vis spectrophotometer in the range of 300–800 nm wavelength to confirm the results observed visually. The results obtained by UV-Vis spectroscopy revealed the formation of absorption peaks at ~540 nm (Fig. 2), which signified the formation of AuNPs in the reaction mixtures, suggesting the justification for the reduction of Au^{3+} to Au^0.[35,36] Compounds such as eugenol, caryophyllene, and benzene-1,2-dimethoxy-4-1-propenyl may play a profound role in the reduction of $HAuCl_4$ to gold nanoparticles.

A broad and sharp band was observed at approximately 540 nm, corresponding to the SPR band of the Os-AuNPs. Several groups have reported similar spectral bands for green-synthesised AuNPs.[23,37,38] The occurrence of a broad and single spectral band during scanning in the range of 300–800 nm was attributed to the synthesis of monodisperse and homogenous AuNPs.

To further validate the morphology and UV spectroscopy results, essential oil-synthesised Os-AuNPs were subjected to DLS analysis. Fig. 3 shows the characteristic size and charge of the synthesised Os-AuNPs using DLS which provided an overall inference of the hydrodynamic diameter of the prepared AuNPs. The *Z*-average size was found to be 57.81 nm, and the polydisparity index (PDI) was 0.42. PDI values below 1 were considered good, indicating that the synthesised Os-AuNPs did not auto-aggregate when dispersed in an aqueous solution. Hence, the *Z*-average size and PDI values correlated well with the results obtained through UV-visible spectroscopy, thus exhibiting a homogenous distribution of nanoparticles formed during the green synthesis route. The zeta potential of Os-AuNPs was found to be −27.6 mV: the higher the surface zeta potential, the greater their overall stability. Modulation of the surface zeta potential is crucial for developing nanoparticles which can be targeted for specific drug delivery.

SEM and TEM images of the synthesised Os-AuNPs are shown in Fig. 4. The SEM images provided a rough estimate of the overall shape of the synthesised nanoparticles (Fig. 4a) which was further confirmed by the TEM images. The TEM measurements shed light on the morphology and particle size of the green-synthesised Os-AuNPs. However, during green synthesis, many gold nanostructures, such as triangles and tetrahedrons, were formed. The TEM micrographs revealed that the synthesised Os-AuNPs were in the range of 14–54 nm, with an overall average size range of 24 to 28 nm (Fig. 4b). The bottom-up synthesis of the anisotropic structures in AuNPs clearly indicates that, owing to the reaction mixtures using essential oils[39] and associated metabolites in the mixture solution, the plant products acted as a predominant capping agent for the formation of the anisotropic structures[40] of AuNPs. Different plant metabolites, especially the associated essential oils present in Tulsi plant extracts, act as directional capping

Retention time	Compounds name	Molecular formula	Molecular weight
20.76	Eugenol	$C_{10}H_{12}O_2$	164.3
21.85	Benzene-1,2-dimethoxy-4-1 propenyl	$C_{11}H_{14}O_2$	178.3
22.15	Caryophyllene	$C_{15}H_{24}$	204.4

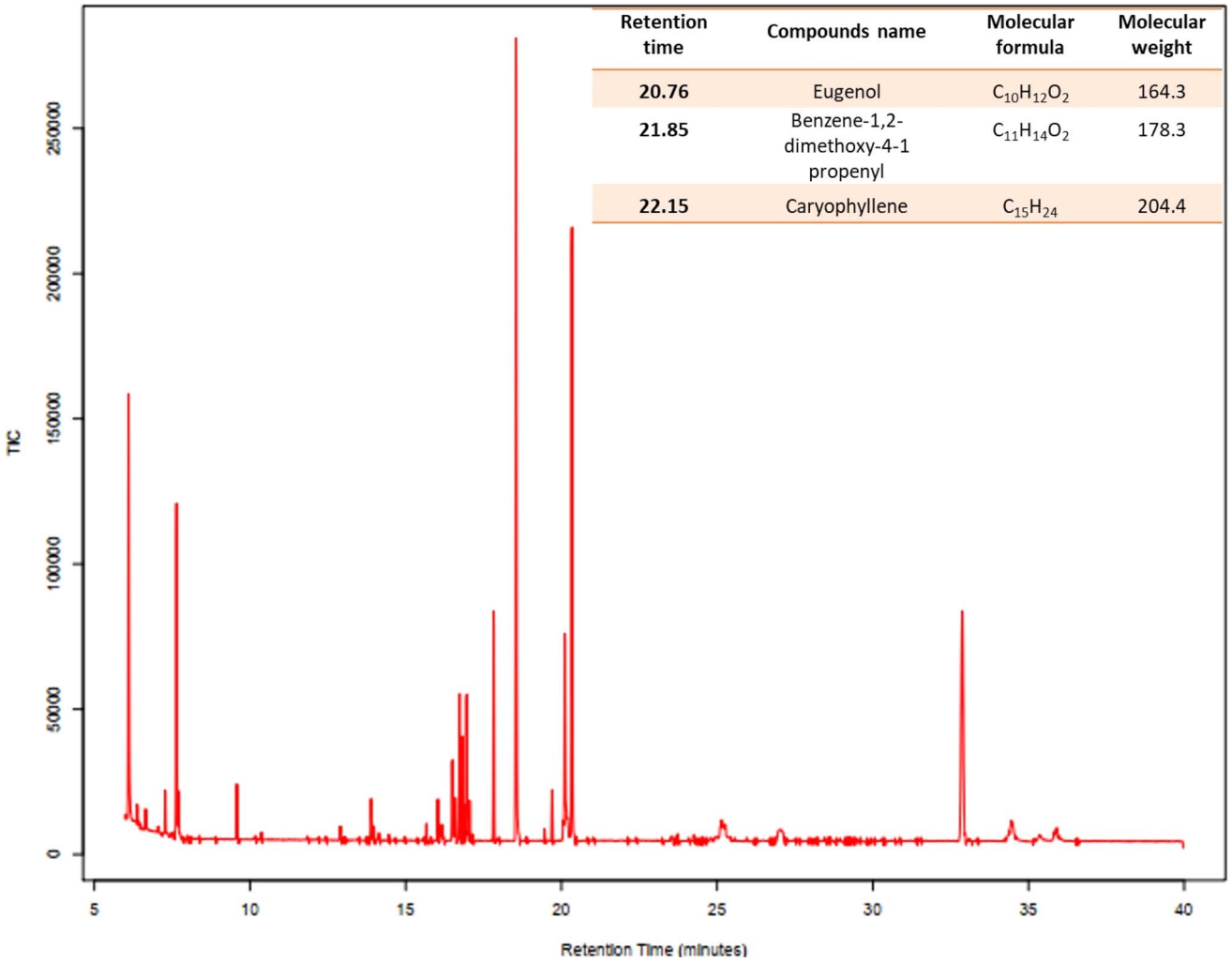

Fig. 1 GC-MS spectral peaks of the *O. sanctum* essential oil extract.

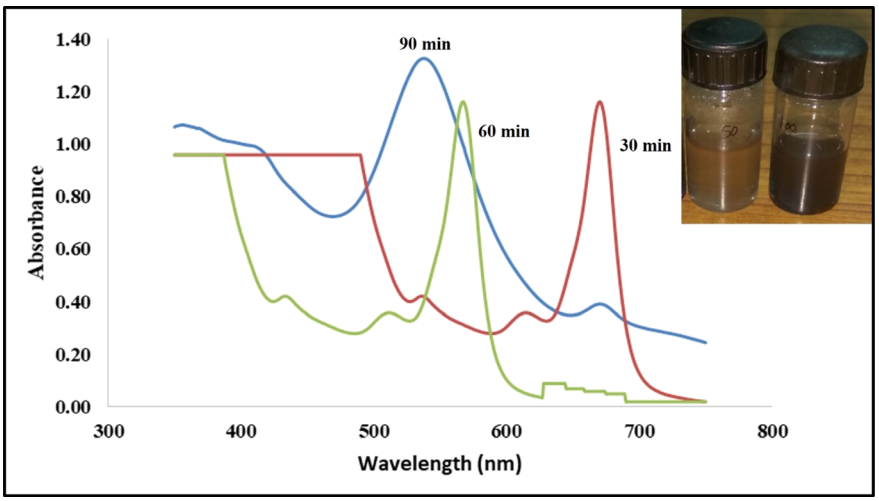

Fig. 2 UV-visible absorption bands and visual color change inference (inset) of the green synthesized Os-AuNPs mediated through the oil extracts of *O. sanctum*.

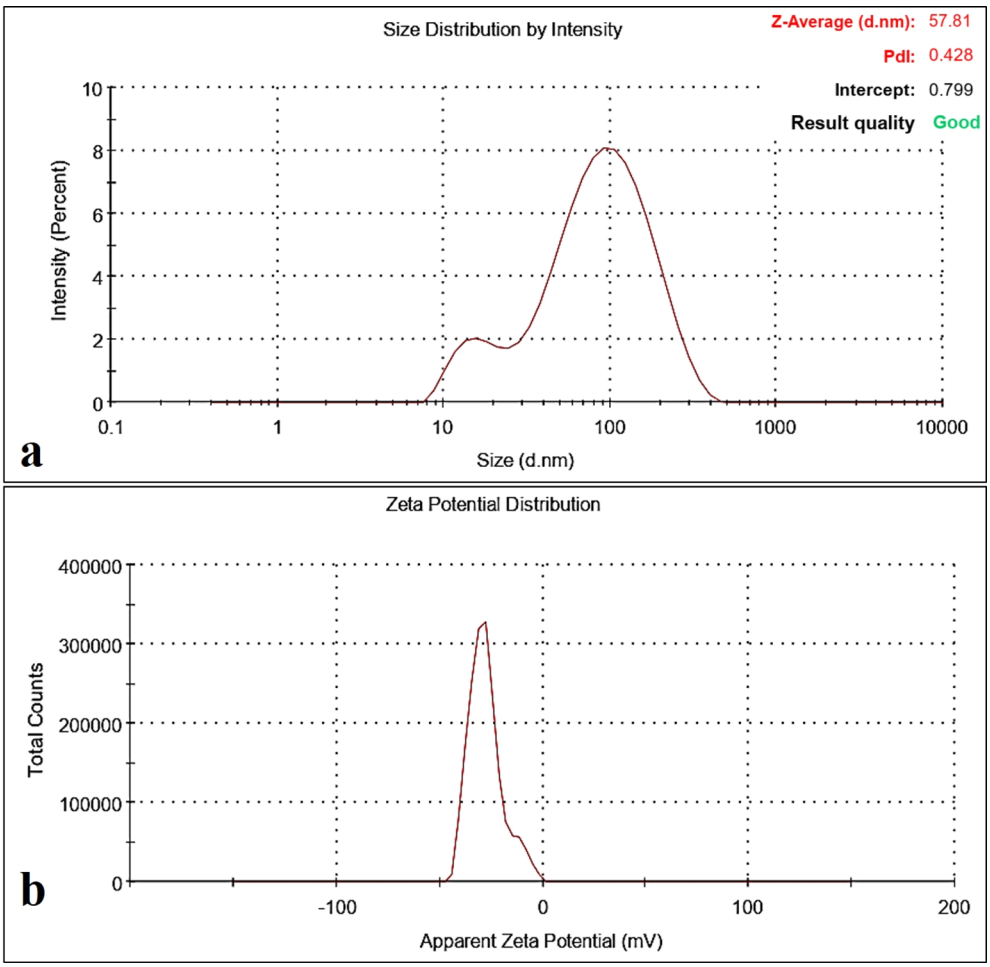

Fig. 3 Dynamic light scattering studies characterizations of the synthesized Os-AuNPs mediated through the oil extracts of *O. sanctum* (a) hydrodynamic diameter (*Z*-average size); (b) surface zeta potential (mV).

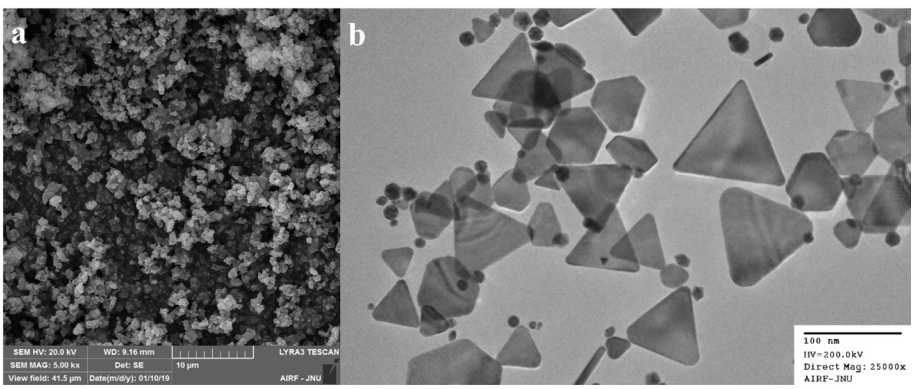

Fig. 4 Electron microscopy of the synthesized Os-AuNPs observed through (a) SEM; (b) TEM.

elements that dictate the dynamics and directional formation of differently shaped (from spherical to prismatic) edged AuNPs in solution. Such anisotropic AuNP formation plays a critical role in eliciting robust anti-microbial and anti-cancerous activities under *in vitro* conditions owing to the presence of surface edges[41] in their structures, which aids in achieving the desired penetration and percolation properties in targeted biological systems.

Fig. 5a shows the diffraction pattern of green-synthesised Os-AuNPs. Major XRD patterns were observed at the lattice planes of 27.32°, 36.72°, 42.90°, 63.25°, and 76.38° lattice, which are in accordance with the standard pattern JCPDS-04-0783 database. The XRD patterns illustrate the synthesis of the face-centred

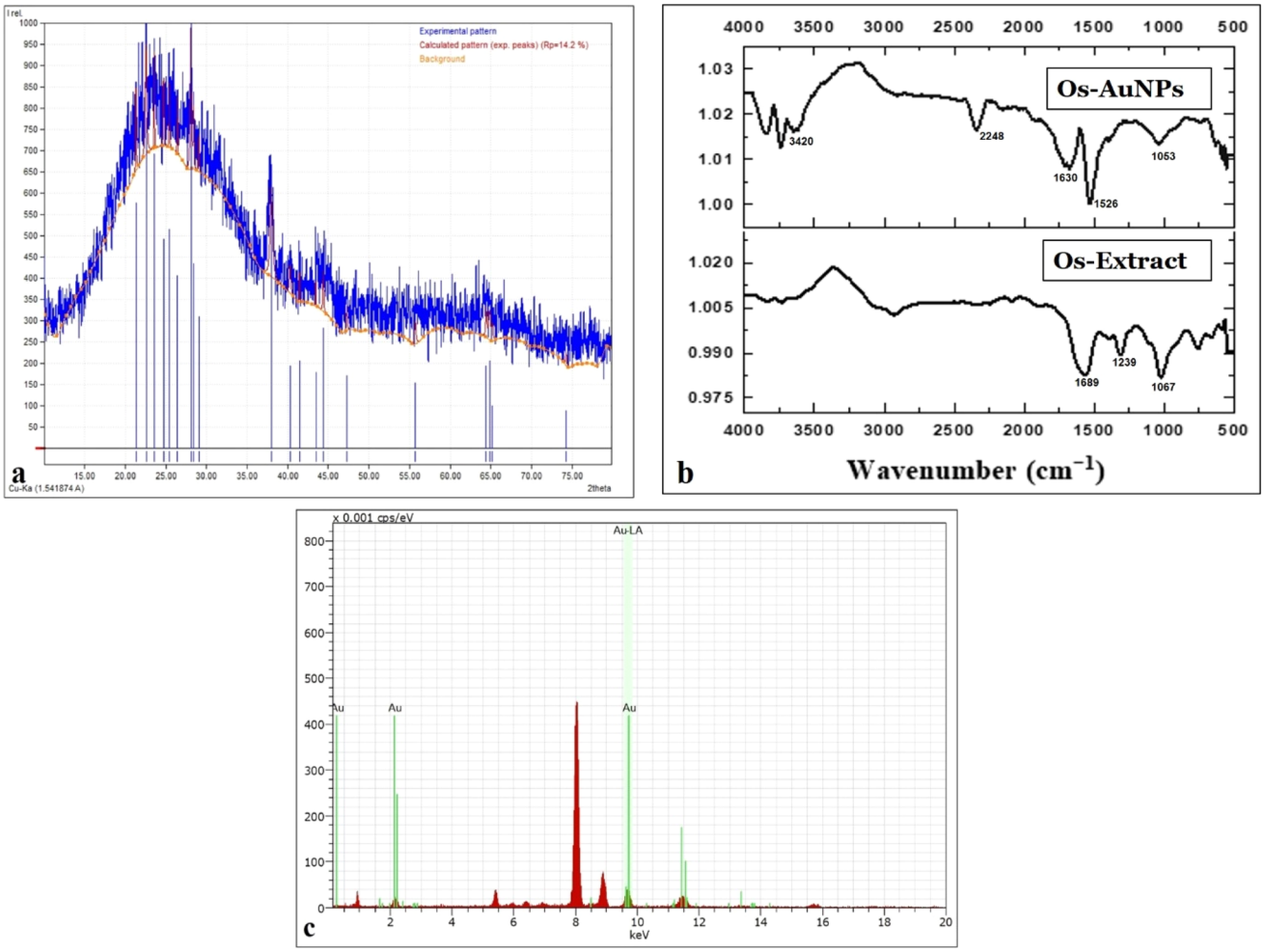

Fig. 5 Characteristic studies of the green synthesized Os-AuNPs (a) XRD diffractogram; (b) FTIR spectrum; (c) EDX.

cubic crystal structure of the Os-AuNPs. Such crystallinity in the as-prepared AuNPs[42] resulted in the display of potential antibacterial and anticancer activities under *in vitro* conditions owing to their surface modulations and grain size. The crystallinity of nanoparticles determines the sharper edges during the bottom-up formation of particles, which causes different reactions with biological systems to achieve myriad therapeutic activities.

The FT-IR spectra of the synthesised Os-AuNPs were recorded to determine the biomolecules responsible for metal ion bio-reduction and NP encapsulation. Fig. 5b shows the ATR-FTIR spectral bands of the Os-AuNPs scanned in the range of 500–4000 cm^{-1}. The spectra of different vibration modes were centred at 1053.8, 1160.9, 1239, 1384.4, 1497.3, 1,526, 1630.3, 2248, and 3420 cm^{-1} owing to the presence of various vibrations, such as C═O stretching vibrations (presence of amide I group), N–O, –C═C, –C═O (presence of carboxylic acids and carbonyl groups), and C–N (presence of aliphatic amine groups). Furthermore, the occurrence of broad bands suggested the presence of phenolic groups (O–H stretching) and aromatic rings (C–O groups). *Ocimum* species are rich in many polyphenolic components, such as caffeic acid, luteolin, aesculin, and chlorogenic acid. During nanoparticle synthesis, the polyphenolic compounds present in the essential oil extract may reduce $HAuCl_4$ *via* an oxidation–reduction reaction. Similar results have been reported by various groups for green-synthesised AuNPs.[43,44]

Fig. 5c shows the EDX spectra of the synthesised Os-AuNPs. At ~1.5 keV the EDX spectrum indicated the presence of elemental gold which was possibly due to the bioreduction of the precursor $HAuCl_4$ to AuNPs. Furthermore, the weak oxygen peaks may be due to the surface adsorption of biomolecules during the synthesis of Os-AuNPs.

Biocompatibility with blood components is essential for the development of new pharmaceutical formulations. Blood is the lifeline of our body, and any compound administered must pass through hemolysis and hemagglutination tests. Fig. 6 shows the hemolytic activity of the green-synthesised Os-AuNPs and Os extract. From Fig. 5a, one can clearly observe that the synthesised Os-AuNPs exhibited negligible hemotoxicity towards haemoglobin. Furthermore, the hemagglutination assay (Fig. 6b) showed that, with subsequent dilution, button-like structures were observed in the blood and nanoparticle interaction wells. Clear round button-like structures could be seen in

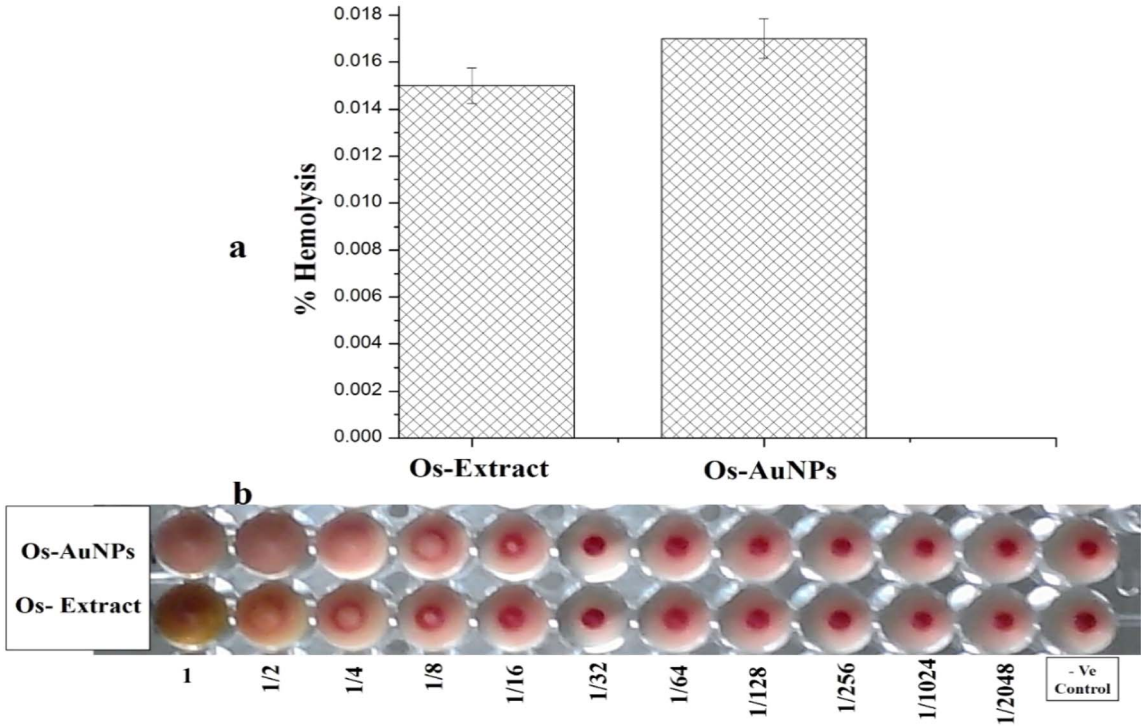

Fig. 6 Hemocompatibility assays of the green synthesized OS-AuNPs (a) hemolysis activity; (b) hemagglutination activity.

the 4th well, whereas in the Os extracts, they were visible in the 2nd well itself. According to ISO/TR 7406, for biomaterial application, >5% hemolysis value is considered safe for use.[28] Hence, from the observed results, it is clear that the synthesised OS-AuNPs exhibited negligible hemolysis with blood corpuscles and were thus biocompatible in nature.

3.3. Antibacterial activities

The antibacterial effect of green-synthesised AuNPs against a wide range of pathogenic species was anticipated in this study. Preliminary studies using an agar well diffusion assay revealed zones of inhibition (ZI) against nosocomial bacterial strains. *Ocimum sanctum* essential oil-functionalized AuNPs exhibited potential antibacterial activity against human pathogenic bacteria, thus affirming that Os-AuNPs are promising antibacterial agents. The screening results (ZIs) served as the basis for further examination of AuNPs against individual pathogens using a microbroth dilution method. The MIC values of the Os-AuNPs for each pathogenic bacterial strain are shown in Fig. 7.

The IC_{50} values observed in the microbroth dilution assay indicated strong antimicrobial activity of the synthesised Os-AuNPs. MIC values of 17.37 ± 0.67, 42.09 ± 0.47, 58.52 ± 0.37 and 34.65 ± 1.47 μg mL^{-1} was observed against *P. aeruginosa*, *E. coli*, *V. cholera* and *B. subtilis*, respectively. Gentamycin a widely used antibiotic was used as positive control for the above antimicrobial test against the pathogenic test microorganisms. The precise mechanism and reactive species involved in the bactericidal action of nanoparticles such as AuNPs or liberated Au^+, are not well established and continue to be a topic of discussion. However, recent investigations have shown that the released Au^+, and not the actual AuNPs themselves, may be the antimicrobial agent responsible for causing cell damage and, ultimately, death. The generation of reactive oxygen species, free radicals derived from the surface of AuNPs, gold ion stress, coating agents, and interactions with bacterial cells can lead to depletion of intracellular ATP levels. Damage to respiratory enzymes is one of the pathways proposed for the bactericidal activity of AuNPs.

The higher the surface area of the AuNPs in contact with the bacterial membrane, the more potent their bactericidal action.

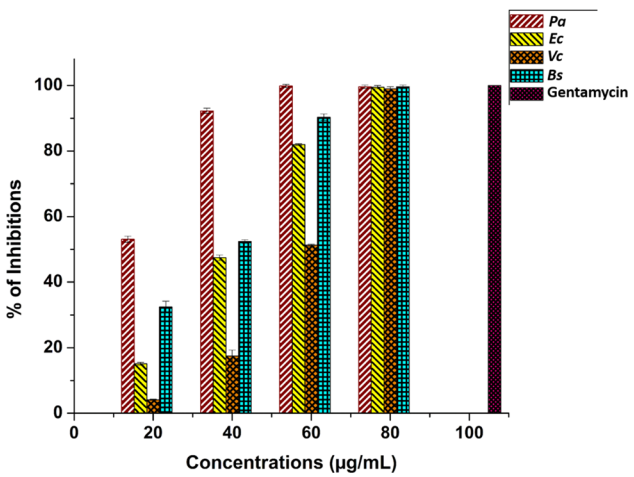

Fig. 7 Minimum inhibitory concentrations of Os-AuNPs against *P. aeruginosa*, *E. coli*, *V. cholerae* and *B. subtilis* ($p \leq 0.05$) and standard antibiotic Gentamycin as control.

The cell shape is altered because of the repulsion between the positively charged Au ions and negatively charged cell membranes, resulting in leakage and eventual cell death. Hence, AuNPs kill bacteria by increasing the permeability of their membranes, which is accomplished by generating pores or pits in the cell walls.

3.4. MTT assay

The MTT cell cytotoxicity assay relies on the activity of the oxidoreductase enzyme present in the mitochondria to reduce the MTT dye to an insoluble formazan product, and the amount of formazan produced determines the rate of cellular metabolism.[45] Hence, intact cells produce more formazan than dead cells. Therefore, theoretically, Os-AuNP-treated MCF-7 breast carcinoma cells should produce less formazan than untreated control cells. Fig. 8i depicts the % cell viability of MCF-7 breast carcinoma cells treated with standard cisplatin, Os extract, and green-synthesised Os-AuNPs. Os-extracts and Os-AuNPs demonstrated dose-dependent cytotoxicity with IC_{50} values of 71.29 ± 3.2 and 78.51 ± 2.4 μg mL^{-1} respectively. The *Ocimum* extract exhibited a statistically significant difference in toxicity, as demonstrated by the Os-AuNPs. Various groups have reported similar results using AuNPs against HCT-116, MCF-7, A549, and RAW264.7 cancer cells, which correlated with our current observation of green-synthesised AuNPs.[46–50]

The cell cycle is a complex process governed by various checkpoint mechanisms. During mutation or stress conditions, cells are further restricted from synthesising mutated genetic material.[51] In cancer, this restriction is completely absent, as most of the checkpoint signalling cascades themselves are mutated, resulting in unconditional growth potentials forming tumorous outgrowth. Cell cycle analysis was performed using flow cytometry after treating MCF-7 breast carcinoma cells with the Os-extract and Os-AuNPs, with the standard drug cisplatin as a positive control (Fig. 8ii). Under *in vitro* conditions, cancer cells treated with Os-extracts and Os-AuNPs exhibited chromosomal instability and mitotic arrest. This was evident from the

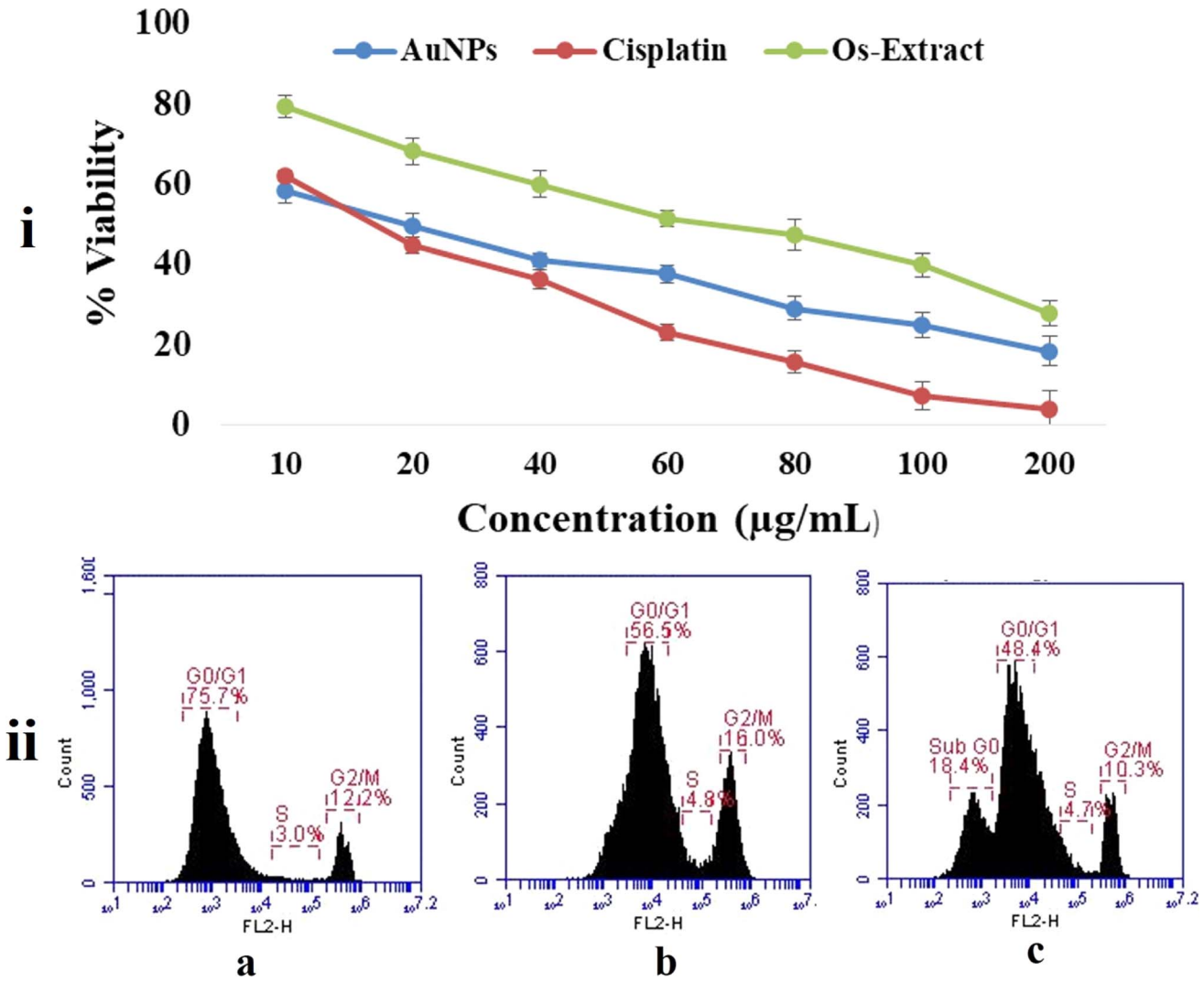

Fig. 8 Cell cytotoxicity assay performed against MCF-7 breast carcinoma cell lines after treatment with green synthesized Os-AuNPs (i) MTT assay; (ii) cell cycle analysis using flow cytometry (a) cisplatin treated cells; (b) Os-extract treated cells; (c) Os-AuNPs treated cells.

G2/M phase expression profile and the intensity of the S phase. Compared with the control group, the Os-extract and Os-AuNPs exhibited 16.0% and 10.3% G2/M phases, respectively, and both samples were effective in controlling the S phase at 4.89 and 4.7%. The sub G0 phase, indicating apoptotic cells, was observed in Os-AuNP-treated cells at approximately 18.45, indicating that the synthesised Os-AuNPs had the potential to induce apoptosis in MCF-7 breast carcinoma cells.

Reactive oxygen species (ROS) are produced naturally in cells and instigate various biochemical pathways; however, excessive production of ROS can induce pathological conditions leading to cancer cell development.[52] Various reports have documented the efficiency of AuNPs in initiating intracellular ROS.[53,54] Fig. 9 shows the intracellular production of ROS after treatment with the Os extracts and Os-AuNPs. DCFH-DA efficiently indicated the overall accumulation of H_2O_2, OH–, carbonate radicals, and NO in the cells. Upon contact with ROS, the non-fluorescent dye becomes sensitive and produces fluorescence which ultimately results in increased fluorescence in ROS-generating cells. Fig. 9a shows the fluorescence intensity of the DCFH-DA dye using flow cytometry, where higher-intensity peaks indicate higher ROS generation in Os-AuNP-treated cells than in Os-extract-treated cells. Similarly, higher fluorescence intensity of the cells indicated higher ROS production in the fluorescence microscopy images (Fig. 9b) than in the untreated control cells.

Fig. 10 exhibits the fluorescence intensity of rhodamine 123 using flow cytometry and fluorescence microscopy images. Any change in the mitochondrial membrane potential can disrupt the electron transport chain, which can be harmful to cells. Rhodamine 123 stains the mitochondria; therefore, intact cells produce more fluorescence than dead cells. Fig. 10a clearly shows that the fluorescence intensity measured by flow cytometry in untreated control cells was higher than that in the Os-extract- and Os-AuNP-treated cells. Fluorescence microscopy yielded similar results (Fig. 10b). Hence, it can be inferred that the synthesised Os-AuNPs trigger intracellular ROS production which depolarises and regulates the mitochondrial permeability transition pore complex (PTPC). This facilitates the invasion of free radicals and solutes which target mitochondrial DNA, thereby disturbing the transcriptional and cellular harmony inside the cell. Mitochondrial damage directly affects ATP formation and prevents cellular energy depletion. The Rhodamine 123 assay visually demonstrated that Os-AuNPs and Os extracts trigger intracellular ROS that ultimately leads to altered $\Delta\Psi_m$ which facilitates a probable apoptotic cell death mechanism.

Cell cycle analysis and mitochondrial membrane potential studies provided a strong signal for the apoptotic cell death pathway in Os-AuNP- and Os-extract-treated MCF-7 cells. Hence, to validate the possible role of the anticancer mechanism facilitated by green-synthesised Os-AuNPs through apoptosis or necrosis, an Annexin V-FITC assay was performed (Fig. 11). Annexins are a family of calcium-dependent phospholipid-binding proteins which bind to phosphatidylserine on the cell membrane to induce apoptosis. Phosphatidylserine is the basic component of the cell membrane and remains in the inner wall of the cytoplasm of healthy cells. During cell membrane damage, phosphatidylserine residues are exposed on the outer surface. Hence, Annexin V binds easily to this exposed layer of phosphatidylserine and provides an indication of the onset of apoptosis. As shown in Fig. 11, the % of dead cells was higher in Os-AuNP-treated cells (Fig. 11b) than in Os-extract-treated cells (Fig. 11a). Similar results were previously reported by Nayak *et al.* using green-synthesised AgNPs against skin carcinoma and osteosarcoma.[55,56]

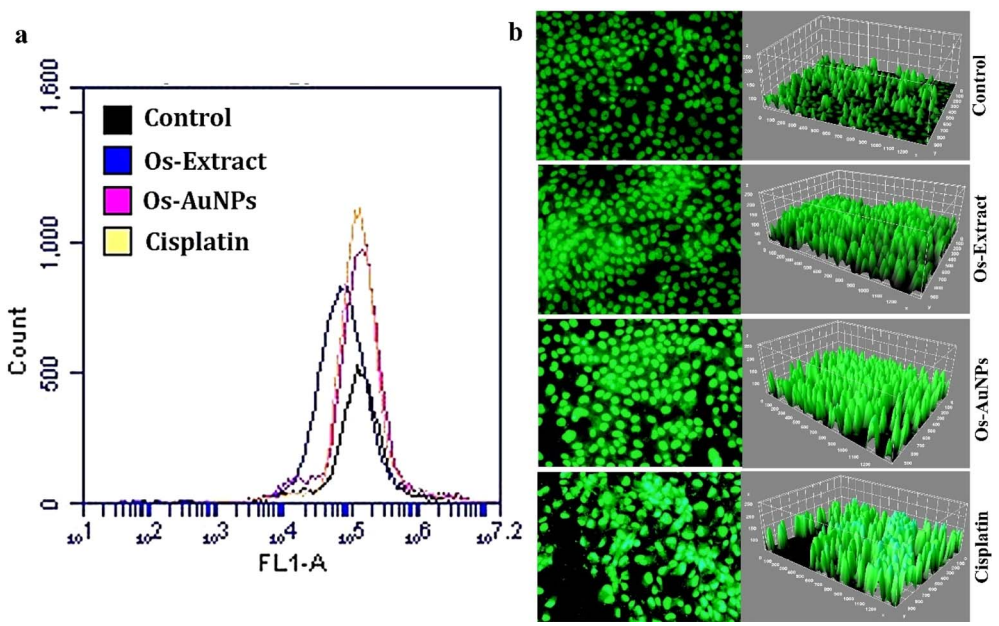

Fig. 9 Intracellular ROS production activity detected through (a) flow cytometry using FL1 filter; (b) fluorescence microscopy images analyzed through ImageJ software.

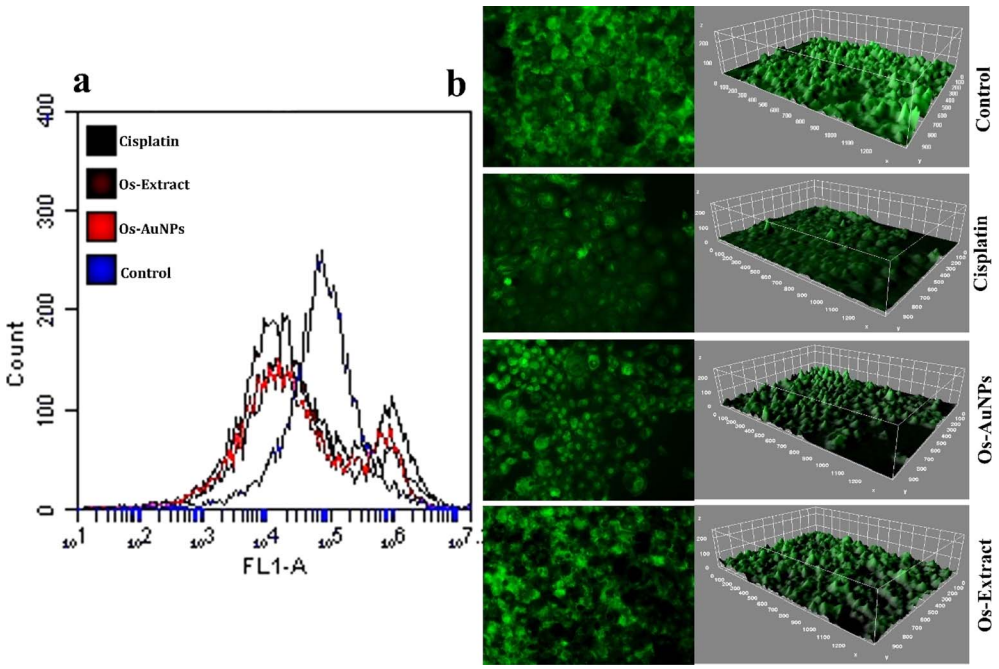

Fig. 10 Mitochondrial membrane potential studies using Rhodamine 123 dye: (a) flow cytometric analysis through FL 1 filter; (b) fluorescence microscopy images analyzed through image J software.

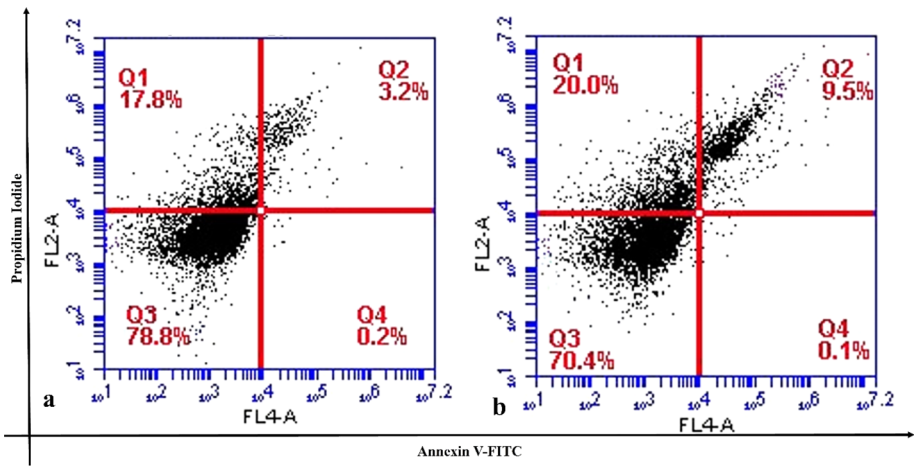

Fig. 11 Annexin V-FITC studies (a) Os-extract treated cells; (b) Os-AuNPs treated cells.

As previous experiments of the Annexin V-FITC assay demonstrated the possible role of Os-AuNPs in exerting apoptotic pathways for their anticancer potential, DNA damage studies were performed to visualise the fragmentation of cellular DNA through agarose gel electrophoresis. Fig. 12a shows the fragmented DNA patterns of the Os-extract- and Os-AuNP-treated MCF-7 cells. DNA smear-like pattern formation has generally been reported in nanoparticle-treated cells.[44,57] To confirm our results, DNA damage studies were performed at the single-cell level using a comet assay. Fig. 12b shows the comets formed by fluorescence spectroscopy after treatment with the synthesised Os-AuNPs and Os extracts. Some important comet parameters, such as comet tail length, comet tail intensity, and comet olive tail movement, were analysed using the openComet plugin of ImageJ software (Fig. 12c). These three parameters provide insight into the movement of DNA in relation to the intensity of fragmentation upon its interaction with nanoparticles and are considered statistically significant measurements.[24]

The colony-forming potential of MCF-7 cells upon incubation with Os-AuNPs and Os-extracts is shown in Fig. 13. After 14 days of incubation, the number of cells in the control group increased exponentially, whereas in the AuNP- and extract-treated groups, the number decreased. Hence, this assay offers an indirect assessment that our synthesised nanoparticles were effective in restricting the aggressive growth

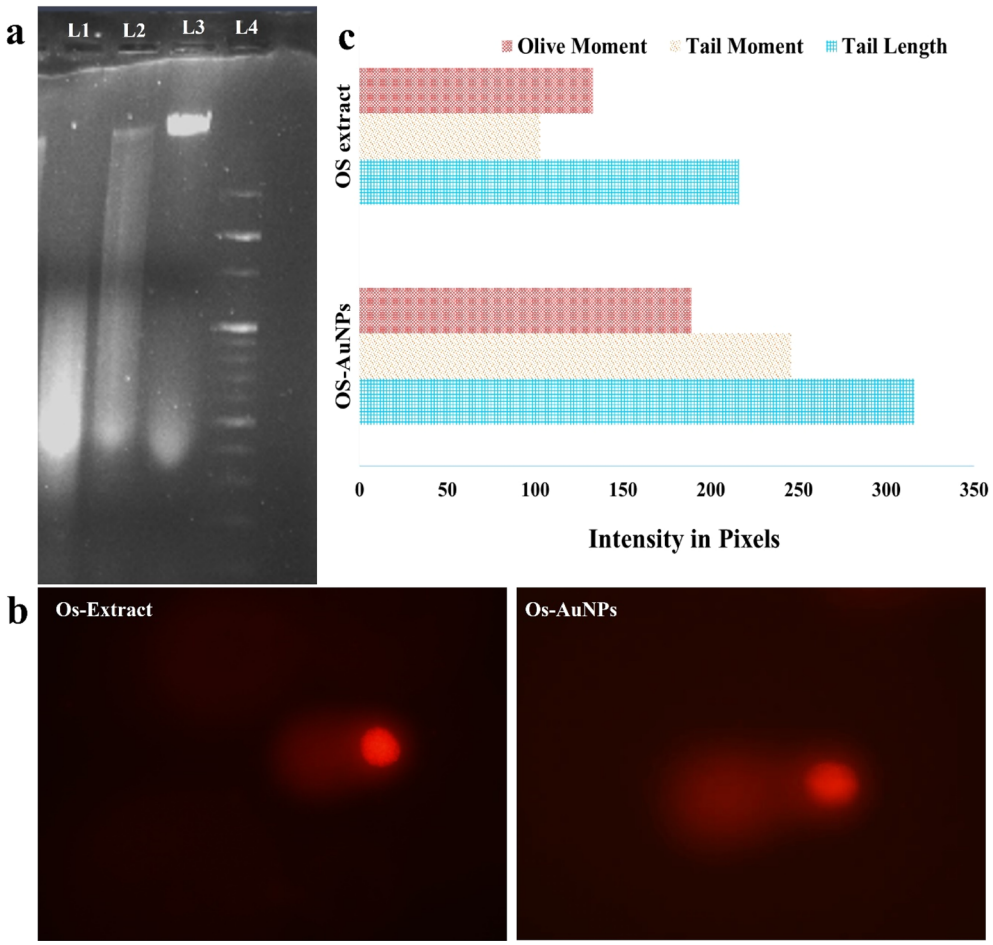

Fig. 12 DNA damage studies: (a) agarose gel electrophoresis where the lane L1, L2, L3 and L4 represents the Os-AuNPs, Os-extracts, control and DNA ladder respectively; (b) fluorescence images of Comets formed; (c) olive moment, tail moment and tail length analysis through opencomet plugin of ImageJ software.

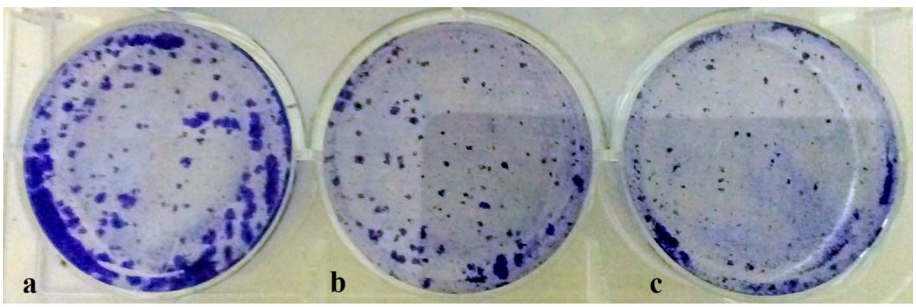

Fig. 13 Colony forming assay of the MCF-7 treated cells (a) control cells; (b) Os-extract treated cells; (c) Os-AuNPs treated cells.

potential of cancerous cells which is in agreement with our previously discussed experimental results.[58]

4 Conclusion

Ocimum gold nanoparticles have been introduced as medicinally important entities using renewable extracts. The polyphenolic components of the extract serve as potential reducing and stabilising agents. The scanning and transmission electron microscopy images demonstrated the triangular shaped AuNPs. GC-MS and FTIR spectral analysis of AuNPs revealed a plethora of bioactive compounds and functional groups associated with particle synthesis that are responsible for metabolomic activities. The presence of multiple compounds in Os-AuNPs is endowed with beneficial attributes responsible for the antimicrobial activities against the nosocomial *P. aeruginosa E. coli*, *V.*

cholerae, and *B. subtilis* strains. The MTT and cell cycle analysis of the synthesized AuNPs illustrated the dose dependent cytotoxicity endowered upon the MCF-7 breast carcinoma cells. Subsequent studies revealed their ROS inducing capabilities thereby instigating a cascade of events to strategically destabilize the mitochondrial membrane potential. The change in membrane potential thus hampers the cellular harmony and cell membrane integrity. The ethnomedicinal significance of *Ocimum* gold nanoparticles is enormous, and the results will be of enormous help for nanotechnological and biochemical applications. These findings also support the use of environmentally friendly AuNP synthesis methods that utilise bio activating chemicals as reducers. Thus, further research on synthesis procedure enhancement and optimisation is critical for improving the bottom-up green synthesis approach for functionalized nanoparticle synthesis and fabrication on a large scale. Such refined strategies for the green synthesis of AuNPs can avoid the toxicities associated with the conventional chemical route of AuNPs and assist in biocompatible production and applications in the biomedical domain.

Ethical approval

No animals were used in this study.

Data availability

The research article data were generated using laboratory conditions and the analyses were done through Origin Software. The GC/MS data were compared with the GC/MS database. Data for this article, including figures and graphs are available from the corresponding authors: Dr Debasis Nayak (deb63-nayak@gmail.com) and Dr Bibhu Prasad Panda (bibhuprasadpanda@soa.ac.in/bibhuprasadpanda14@gmail.com)).

Author contributions

Y. K. M., K. B., A. K. M., and D. N. conceptualised and designed the experiments and wrote the manuscript. B. P. S. K. A and B. M. analysed the characterisation data and revised the manuscript. Y. K. M., J. P., S. K. A, and B. P. P. collected data and wrote, prepared illustrations, reviewed, and edited the manuscript. All data were generated in-house, and no paper mill was used. All authors agree to be accountable for all aspects of this study and to ensure its integrity and accuracy. All authors have read and approved the final manuscript.

Conflicts of interest

The authors declare that there are no conflicts of interest among the authors of this manuscript or other research groups.

Acknowledgements

The authors are thankful to their respective institutions for providing research facilities for this work.

References

1 A. Bishayee and G. Sethi, Bioactive natural products in cancer prevention and therapy: Progress and promise, *Semin. Cancer Biol.*, 2016, 1–3.
2 H. Wang, T. Oo Khor, L. Shu, Z.-Y. Su, F. Fuentes, J.-H. Lee, *et al.*, Plants *vs.* cancer: a review on natural phytochemicals in preventing and treating cancers and their druggability, *Anti-Cancer Agents Med. Chem.*, 2012, **12**(10), 1281–1305.
3 B. Holst and G. Williamson, Nutrients and phytochemicals: from bioavailability to bioefficacy beyond antioxidants, *Curr. Opin. Biotechnol.*, 2008, **19**(2), 73–82.
4 M. Khatami, F. Mosazade, M. Raeisi, M. Ghasemi, Z. Fazli, K. Arefkia, *et al.*, Simplification of gold nanoparticle synthesis with low cytotoxicity using a greener approach: opening up new possibilities, *RSC Adv.*, 2021, **11**(6), 3288–3294.
5 R. H. Liu, Health benefits of fruit and vegetables are from additive and synergistic combinations of phytochemicals, *Am. J. Clin. Nutr.*, 2003, **78**(3), 517S–520S.
6 Y. K. Mohanta, K. Biswas, S. K. Panda, J. Bandyopadhyay, D. De, R. Jayabalan, *et al.*, Phyto-assisted synthesis of biofunctionalised silver nanoparticles and their potential antioxidant, anti-microbial and wound healing activities, *IET Nanobiotechnol.*, 2017, **11**(8), 1027–1034.
7 M. N. Nadagouda, N. Iyanna, J. Lalley, C. Han, D. D. Dionysiou and R. S. Varma, Synthesis of silver and gold nanoparticles using antioxidants from blackberry, blueberry, pomegranate, and turmeric extracts, *ACS Sustain. Chem. Eng.*, 2014, **2**(7), 1717–1723.
8 G. Carrillo-Galván, R. Bye, L. E. Eguiarte, S. Cristians, P. Pérez-López, F. Vergara-Silva, *et al.*, Domestication of aromatic medicinal plants in Mexico: Agastache (Lamiaceae)- A n ethnobotanical, morpho-physiological, and phytochemical analysis, *J. Ethnobiol. Ethnomed.*, 2020, **16**(1), 1–16.
9 G. Castellino, F. Mesa, F. Cappello, C. Benavides-Reyes, G. A. Malfa, I. Cabello, *et al.*, Effects of essential oils and selected compounds from Lamiaceae family as adjutants on the treatment of subjects with periodontitis and cardiovascular risk, *Appl. Sci.*, 2021, **11**(20), 9563.
10 M. A. Hanif, S. Nisar, G. S. Khan, Z. Mushtaq and M. Zubair, Essential oils, in *Essential Oil Research*, Springer, 2019, pp. 3–17.
11 F. Bakkali, S. Averbeck, D. Averbeck and M. Idaomar, Biological effects of essential oils–a review, *Food Chem. Toxicol.*, 2008, **46**(2), 446–475.
12 M. Wink, Plant secondary metabolites modulate insect behavior-steps toward addiction?, *Front. Physiol.*, 2018, **9**, 364.
13 R. R. Raja, Medicinally potential plants of Labiatae (Lamiaceae) family: an overview, *Res. J. Med. Plant*, 2012, **6**(3), 203–213.
14 U. Özgen, A. Mavi, Z. Terzi, M. Coşkun and P. J. Houghton, Antioxidant properties of some medicinal Lamiaceae (Labiatae) species, *Pharm. Biol.*, 2006, **44**(2), 107–112.

15 R. Kumar, P. Saha, P. Lokare, K. Datta, P. Selvakumar and A. Chourasia, A Systemic Review of Ocimum sanctum (Tulsi): Morphological Characteristics, Phytoconstituents and Therapeutic Applications, *Int. J. Res. Appl. Sci. Biotechnol.*, 2022, **9**(2), 221–226.

16 N. Bano, A. Ahmed, M. Tanveer, G. M. Khan and M. T. Ansari, Pharmacological evaluation of Ocimum sanctum, *J. Bioequivalence Bioavailability*, 2017, **9**(3), 387–392.

17 S. Mondal, B. R. Mirdha and S. C. Mahapatra, The science behind sacredness of Tulsi (Ocimum sanctum Linn.), *Indian J. Physiol. Pharmacol.*, 2009, **53**(4), 291–306.

18 K. V. Kulkarni and B. V. Adavirao, A review on: Indian traditional shrub Tulsi (Ocimum sanctum): the unique medicinal plant, *J. Med. Plants Stud.*, 2018, **6**(2), 106–110.

19 Y. Shah and K. Shah, Anti-viral herbal phytoconstituents of tulsi (Ocimum sanctum) against Covid-19, *IP Int. J. Compr. Adv. Pharmacol.*, 2022, **7**(2), 77–80.

20 D. Jindal and V. Rani, In Silico Studies of Phytoconstituents from Piper longum and Ocimum sanctum as ACE2 and TMRSS2 Inhibitors: Strategies to Combat COVID-19, *Appl. Biochem. Biotechnol.*, 2022, 1–18.

21 S. Sharma, D. Singh, K. P. Seema, R. K. Gupta, S. J. Ravikant and S. Singh, Therapeutic Role Of Giloy And Tulsi Against Covid-19, *COVID 19 Impact Response*, 2020, vol VI, p. 15.

22 C.-M. J. Hu, S. Aryal and L. Zhang, Nanoparticle-assisted combination therapies for effective cancer treatment, *Ther. Delivery*, 2010, **1**(2), 323–334.

23 P. C. Chen, S. C. Mwakwari and A. K. Oyelere, Gold nanoparticles: from nanomedicine to nanosensing, *Nanotechnol., Sci. Appl.*, 2008, **1**, 45–66.

24 J. M. Rodriguez-Vargas, M. J. Ruiz-Magana, C. Ruiz-Ruiz, J. Majuelos-Melguizo, A. Peralta-Leal, M. I. Rodriguez, *et al.*, ROS-induced DNA damage and PARP-1 are required for optimal induction of starvation-induced autophagy, *Cell Res.*, 2012, **22**(7), 1181–1198.

25 E. M. Banla, D. K. Dzidzienyo, M. M. Diangar, L. D. Melomey, S. K. Offei, P. Tongoona, *et al.*, Molecular and phenotypic diversity of groundnut (Arachis hypogaea L.) cultivars in Togo, *Physiol. Mol. Biol. Plants*, 2020, **26**(7), 1489–1504.

26 A. Prasad, A. Khatua, Y. K. Mohanta, M. Saravanan, R. Meena and I. Ghosh, Low-Dose Exposure of Photosynthesized Gold Nanoparticle Combined with Glutamine Deprivation Enhances Cell Death in Cancer Cell line HeLa *via* Oxidative Stress-Mediated Mitochondrial Dysfunction and G0/G1 Cell Cycle Arrest, *Nanoscale*, 2022, **14**, 10399–10417.

27 D. Nayak, N. C. Thathapudi, S. Ashe and B. Nayak, Bioengineered ethosomes encapsulating AgNPs and Tasar silk sericin proteins for non melanoma skin carcinoma (NMSC) as an alternative therapeutics, *Int. J. Pharm.*, 2021, **596**, 120265.

28 M. Weber, H. Steinle, S. Golombek, L. Hann, C. Schlensak, H. P. Wendel, *et al.*, Blood-Contacting Biomaterials: In Vitro Evaluation of the Hemocompatibility, *Front. Bioeng. Biotechnol.*, 2018, **6**, 99.

29 Y. Mohanta, K. Biswas, S. Jena, A. Hashem, E. Abd_Allah and T. Mohanta, Anti-biofilm and Antibacterial Activities of Silver Nanoparticles Synthesized by the Reducing Activity of Phytoconstituents Present in the Indian Medicinal Plants, *Front. Microbiol.*, 2020, **11**, 1–15.

30 D. Sengupta, M. Deb, S. K. Rath, S. Kar, S. Parbin, N. Pradhan, *et al.*, DNA methylation and not H3K4 trimethylation dictates the expression status of miR-152 gene which inhibits migration of breast cancer cells via DNMT1/CDH1 loop, *Exp. Cell Res.*, 2016, **346**(2), 176–187.

31 S. Kar, D. Sengupta, M. Deb, A. Shilpi, S. Parbin, S. K. Rath, *et al.*, Expression profiling of DNA methylation-mediated epigenetic gene-silencing factors in breast cancer, *Clin. Epigenet.*, 2014, **6**(1), 1.

32 A. R. Gliga, S. Skoglund, I. O. Wallinder, B. Fadeel and H. L. Karlsson, Size-dependent cytotoxicity of silver nanoparticles in human lung cells: the role of cellular uptake, agglomeration and Ag release, *Part. Fibre Toxicol.*, 2014, **11**(1), 11, available from: **http://particleandfibretoxicology.biomedcentral.com/articles/10.1186/1743-8977-11-11**.

33 D. Nayak, M. Kumari, S. Rajachandar, S. Ashe, N. C. Thathapudi and B. Nayak, Biofilm impeding AgNPs target skin carcinoma by inducing mitochondrial membrane depolarization mediated through ROS production, *ACS Appl. Mater. Interfaces*, 2016, **8**(42), 28538–28553.

34 S. K. Rath, M. Deb, D. Sengupta, V. Kari, S. Kar, S. Parbin, *et al.*, Silencing of ZRF1 impedes survival of estrogen receptor positive MCF-7 cells and potentiates the effect of curcumin, *Tumour Biol.*, 2016, **37**(9), 12535–12546.

35 W. Haiss, N. T. K. Thanh, J. Aveyard and D. G. Fernig, Determination of size and concentration of gold nanoparticles from UV-Vis spectra, *Anal. Chem.*, 2007, **79**(11), 4215–4221.

36 M. Zimbone, L. Calcagno, G. Messina, P. Baeri and G. Compagnini, Dynamic light scattering and UV–vis spectroscopy of gold nanoparticles solution, *Mater. Lett.*, 2011, **65**(19–20), 2906–2909.

37 M. C. Daniel and D. Astruc, Gold Nanoparticles: Assembly, Supramolecular Chemistry, Quantum-Size-Related Properties, and Applications Toward Biology, Catalysis, and Nanotechnology, *Chem. Rev.*, 2004, **104**(1), 293–346.

38 C. R. Patra, R. Bhattacharya, D. Mukhopadhyay and P. Mukherjee, Fabrication of gold nanoparticles for targeted therapy in pancreatic cancer, *Adv. Drug Delivery Rev.*, 2010, **62**, 346–361.

39 A. M. Fayaz, M. Girilal, R. Venkatesan and P. T. Kalaichelvan, Biosynthesis of anisotropic gold nanoparticles using Maduca longifolia extract and their potential in infrared absorption, *Colloids Surf., B*, 2011, **88**(1), 287–291.

40 D. Goyal, A. Saini, G. S. S. Saini and R. Kumar, Green synthesis of anisotropic gold nanoparticles using cinnamon with superior antibacterial activity, *Mater. Res. Express*, 2019, **6**(7), 75043.

41 M. Anandan, G. Poorani, P. Boomi, K. Varunkumar, K. Anand, A. A. Chuturgoon, *et al.*, Green synthesis of anisotropic silver nanoparticles from the aqueous leaf

extract of Dodonaea viscosa with their antibacterial and anticancer activities, *Process Biochem.*, 2019, **80**, 80–88.

42 N. Li, P. Zhao and D. Astruc, Anisotropic gold nanoparticles: synthesis, properties, applications, and toxicity, *Angew. Chem., Int. Ed.*, 2014, **53**(7), 1756–1789.

43 C.-T. Ng, S. T. Dheen, W.-C. G. Yip, C.-N. Ong, B.-H. Bay and L.-Y. Lanry Yung, The induction of epigenetic regulation of PROS1 gene in lung fibroblasts by gold nanoparticles and implications for potential lung injury, *Biomaterials*, 2011, **32**(30), 7609–7615.

44 K. M. Soto, I. Luzardo-Ocampo, J. M. López-Romero, S. Mendoza, G. Loarca-Piña, E. M. Rivera-Muñoz, *et al.*, Gold Nanoparticles Synthesized with Common Mullein (Verbascum thapsus) and Castor Bean (Ricinus communis) Ethanolic Extracts Displayed Antiproliferative Effects and Induced Caspase 3 Activity in Human HT29 and SW480 Cancer Cells, *Pharmaceutics*, 2022, **14**(10), 2069.

45 M. V. Berridge, P. M. Herst and A. S. Tan, Tetrazolium dyes as tools in cell biology: New insights into their cellular reduction, *Biotechnol. Annu. Rev.*, 2005, **11**(SUPPL.), 127–152.

46 S. Akhtar, S. M. Asiri, F. A. Khan, S. T. Gunday, A. Iqbal, N. Alrushaid, *et al.*, Formulation of gold nanoparticles with hibiscus and curcumin extracts induced anti-cancer activity, *Arabian J. Chem.*, 2022, **15**(2), 103594.

47 E. A. Hasan, M. A. El-Hashash, M. K. Zahran and H. M. El-Rafie, Comparative study of chemical composition, antioxidant and anticancer activities of both Turbinaria decurrens Bory methanol extract and its biosynthesized gold nanoparticles, *J. Drug Delivery Sci. Technol.*, 2022, **67**, 103005.

48 M. Hosny, M. Fawzy, Y. A. El-Badry, E. E. Hussein and A. S. Eltaweil, Plant-assisted synthesis of gold nanoparticles for photocatalytic, anticancer, and antioxidant applications, *J. Saudi Chem. Soc.*, 2022, **26**(2), 101419.

49 Z. Yang, Z. Liu, J. Zhu, J. Xu, Y. Pu and Y. Bao, Green synthesis and characterization of gold nanoparticles from Pholiota adiposa and their anticancer effects on hepatic carcinoma, *Drug Delivery*, 2022, **29**(1), 997–1006.

50 B. Nagaraj, S. A. Musthafa, S. Muhammad, G. Munuswamy-Ramanujam, W. J. Chung, H. A. Alodaini, *et al.*, Anti-microbial and anti-cancer activity of gold nanoparticles phytofabricated using clerodin enriched clerodendrum ethanolic leaf extract, *J. King Saud Univ., Sci.*, 2022, **34**(4), 101989.

51 Z. Darzynkiewicz, H. Zhao, Analysis of cell cycle by flow cytometry, *eLS (Encyclopedia of Life Sciences)*, John Wiley & Sons Ltd, Chichester, 2014.

52 B. B. Manshian, C. Pfeiffer, B. Pelaz, T. Heimerl, M. Gallego, M. Möller, *et al.*, High-Content Imaging and Gene Expression Approaches To Unravel the Effect of Surface Functionality on Cellular Interactions of Silver Nanoparticles, *ACS Nano*, 2015, **9**(10), 10431–10444.

53 J. W. Han, S. Gurunathan, J.-K. Jeong, Y.-J. Choi, D.-N. Kwon, J.-K. Park, *et al.*, Oxidative stress mediated cytotoxicity of biologically synthesized silver nanoparticles in human lung epithelial adenocarcinoma cell line, *Nanoscale Res. Lett.*, 2014, **9**(1), 1–14.

54 M. L. Circu and T. Y. Aw, Reactive oxygen species, cellular redox systems, and apoptosis, *Free Radical Biol. Med.*, 2010, **48**(6), 749–762.

55 D. Nayak, S. Pradhan, S. Ashe, P. R. Rauta and B. Nayak, Biologically synthesised silver nanoparticles from three diverse family of plant extracts and their anticancer activity against epidermoid A431 carcinoma, *J. Colloid Interface Sci.*, 2015, **457**, 329–338.

56 S. Ashe, D. Nayak, M. Kumari and B. Nayak, Ameliorating Effects of Green Synthesized Silver Nanoparticles on Glycated End Product Induced Reactive Oxygen Species Production and Cellular Toxicity in Osteogenic Saos-2 Cells, *ACS Appl. Mater. Interfaces*, 2016, **8**(44), 30005–30016.

57 E. Mostafavi, A. Zarepour, H. Barabadi, A. Zarrabi, L. B. Truong and D. Medina-Cruz, Antineoplastic activity of biogenic silver and gold nanoparticles to combat leukemia: beginning a new era in cancer theragnostic, *Biotechnol. Rep.*, 2022, **34**, e00714.

58 J. Wang, H. Zhao, W. Song, M. Gu, Y. Liu, B. Liu, *et al.*, Gold Nanoparticle-Decorated Drug Nanocrystals for Enhancing Anticancer Efficacy and Reversing Drug Resistance Through Chemo-/Photothermal Therapy, *Mol. Pharm.*, 2022, **19**(7), 2518–2534.